Biomech Model Mechanobiol
DOI 10.1007/s10237-015-0741-6

ORIGINAL PAPER

Effect of boundary conditions on yield properties of human femoral trabecular bone

J. Panyasantisuk[1] · **D. H. Pahr**[2] · **P. K. Zysset**[1]

Received: 25 June 2015 / Accepted: 20 October 2015

Abstract Trabecular bone plays an important mechanical role in bone fractures and implant stability. Homogenized nonlinear finite element (FE) analysis of whole bones can deliver improved fracture risk and implant loosening assessment. Such simulations require the knowledge of mechanical properties such as an appropriate yield behavior and criterion for trabecular bone. Identification of a complete yield surface is extremely difficult experimentally but can be achieved in silico by using micro-FE analysis on cubical trabecular volume elements. Nevertheless, the influence of the boundary conditions (BCs), which are applied to such volume elements, on the obtained yield properties remains unknown. Therefore, this study compared homogenized yield properties along 17 load cases of 126 human femoral trabecular cubic specimens computed with classical kinematic uniform BCs (KUBCs) and a new set of mixed uniform BCs, namely periodicity-compatible mixed uniform BCs (PMUBCs). In stress space, PMUBCs lead to 7–72 % lower yield stresses compared to KUBCs. The yield surfaces obtained with both KUBCs and PMUBCs demonstrate a pressure-sensitive ellipsoidal shape. A volume fraction and fabric-based quadric yield function successfully fitted the yield surfaces of both BCs with a correlation coefficient $R^2 \geq 0.93$. As expected, yield strains show only a weak dependency on bone volume fraction and fabric. The role of the two BCs in homogenized FE analysis of whole bones will need to be investigated and validated with experimental results at the whole bone level in future studies.

Keywords Yield criterion · Boundary conditions · Finite element analysis · Trabecular bone · Femur

1 Introduction

Trabecular bone plays an important mechanical role in osteoporosis-related fractures and implant fixation. Among other fractures, hip fractures are most severe (World Health Organization 2003; Sambrook and Cooper 2006). They lead to high morbidity and mortality as well as great personal and socioeconomic costs. Homogenized finite element (FE) analysis can improve bone strength assessment (Dall'Ara et al. 2012, 2013) and implant stability prediction (Steiner et al. 2015), but it requires accurate knowledge of the apparent elastic and yield behavior of trabecular bone. Identifying a complete yield surface necessitates yield points from multiple uniaxial, shear and multiaxial load cases. Additionally, the broad heterogeneity of trabecular bone requires numerous specimens for each load case. Rincón-Kohli and Zysset (2008) performed uniaxial and multiaxial experiments on 110 trabecular bone cylinders, and the yield data fitted to a piecewise generalized Hill criterion. However, in vitro, only a few multiaxial load cases could be performed (Keaveny et al. 1999; Rincón-Kohli and Zysset 2008), and sequential yield tests on the same intact specimen are not possible.

Micro-finite element (μFE) analysis can overcome these limitations (Niebur et al. 2000, 2002). Niebur et al. (2000) developed and validated a simulation technique for trabecular bone yielding using μFE analysis. Thereafter, nonlinear μFE simulations were used in several investigations on various bones (Niebur et al. 2002; Stölken and Kinney 2003; Verhulp

✉ J. Panyasantisuk
jarunan.panyasantisuk@istb.unibe.ch

[1] Institute for Surgical Technology and Biomechanics, University of Bern, Stauffacherstr. 78, 3014 Bern, Switzerland

[2] Institute of Lightweight Design and Structural Biomechanics, Vienna University of Technology, Getreidemarkt 9, 1060 Vienna, Austria

Published online: 30 October 2015

et al. 2008; MacNeil and Boyd 2008). Moreover, yield criteria for human trabecular bone have been assessed by using μFE analysis (Bayraktar et al. 2005; Wolfram et al. 2012; Sanyal et al. 2015). Bayraktar et al. (2005) applied an isotropic modified super-ellipsoid criterion in strain space to 3 human femoral trabecular bone specimens with high volume fraction (BV/TV). Subsequently, Wolfram et al. (2012) successfully identified a BV/TV and fabric-based Tsai–Wu criterion in stress and strain space for 23 human vertebral trabecular samples. However, the data covered a low BV/TV range of 0.06–0.15 and included only vertebral bone. Recently, Sanyal et al. (2015) determined yield properties in 10 human trabecular bone samples from three anatomical sites with a broad range of morphology. They proposed a quartic piecewise-linear criterion that also accounts for trabecular bone density and anisotropy. Nonetheless, the number of samples studied remains small and the definition of yield is different.

In the studies mentioned above, different yield constants were identified according to the shape of a selected yield criterion. Schwiedrzik et al. (2013) introduced a generalized anisotropic quadric yield criterion defined with only 6 parameters. With this criterion, the shape of the yield envelope does not need to be assumed beforehand since its minimization results in the optimal shape among the convex quadrics from a sphere, an ellipsoid to a cone. In addition, the previous studies applied exclusively kinematic uniform boundary conditions. In homogenization theory, boundary conditions (BCs) strongly influence the apparent elastic and post-yield properties of heterogeneous materials (Pahr and Zysset 2008; Panyasantisuk et al. 2015). The three boundary conditions that fulfill Hill's condition for non-periodic random media (Hazanov and Amieur 1995; Ostoja-Starzewski 2006) are:

(a) kinematic uniform BCs (KUBCs), in which the boundary nodes are constrained to displace uniformly;
(b) static uniform BCs (SUBCs), in which the boundary nodes are constrained with uniform traction; and
(c) mixed uniform BCs (MUBCs), which combine uniform displacement and traction constraints.

KUBCs and SUBCs provide, respectively, the upper and lower bounds of the apparent stiffness tensors (Hazanov and Huet 1994), but unfortunately, SUBCs provide a very poor lower bound (Pahr and Zysset 2008). Pahr and Zysset (2008) showed that a set of MUBCs, namely periodicity-compatible MUBCs (PMUBCs), results in effective properties when the cubic volume element faces coincide with orthotropic symmetry planes of the volume element (Pahr and Zysset 2008). Our previous study (Panyasantisuk et al. 2015) compared the elastic behavior of PMUBCs and KUBCs. Our results showed that PMUBCs deliver more compliant elastic properties than KUBCs, and the difference between PMUBCs and KUBCs decreases with increasing BV/TV and fabric eigenvalue. However, the influence of BCs on the yield properties remains unknown.

In this context, the aim of this study is to compare the BV/TV and fabric-based quadric yield properties of femoral trabecular bone obtained by using KUBCs and PMUBCs in a large number of μFE models.

2 Theoretical model

A fabric tensor $\mathbf{M}$ is defined with eigenvalues m_i and eigenvectors $\mathbf{m}_i$ (Cowin 1985; Harrigan et al. 1988) with a normalization $\mathrm{tr}(\mathbf{M}) = 3$.

$$\mathbf{M} = \sum_{i=1}^{3} \mathrm{m}_i \mathbf{M}_i = \sum_{i=1}^{3} \mathrm{m}_i (\mathbf{m}_i \otimes \mathbf{m}_i) \tag{1}$$

A generalized anisotropic quadric yield criterion in stress space (Schwiedrzik et al. 2013) is given by:

$$\mathrm{Y}(\mathbf{S}) := \sqrt{\mathbf{S} : \mathbb{F}\mathbf{S}} + \mathbf{F} : \mathbf{S} - 1 = 0 \tag{2}$$

where $\mathbf{S}$ is the infinitesimal Cauchy stress tensor as only small rotations and small strains are expected for yield at the apparent level. The fourth-order tensor $\mathbb{F}$ and the second-order tensor $\mathbf{F}$ in the case of general orthotropy are expressed with:

$$\mathbb{F} = \sum_{i=1}^{3} \mathrm{F}_{ii}^2 \mathbf{M}_i \otimes \mathbf{M}_i - \sum_{\substack{i,j=1 \\ i \neq j}}^{3} \zeta_{ij} \mathrm{F}_{ii}^2 \mathbf{M}_i \otimes \mathbf{M}_j + \sum_{\substack{i,j=1 \\ i \neq j}}^{3} \frac{\mathrm{F}_{ij}^2}{2} \mathbf{M}_i \underline{\otimes} \mathbf{M}_j \tag{3}$$

$$\mathbf{F} = \sum_{i=1}^{3} \mathrm{f}_i \mathbf{M}_i \tag{4}$$

where

$$\mathrm{F}_{ii} = \frac{\sigma_{ii}^{+} + \sigma_{ii}^{-}}{2\sigma_{ii}^{+}\sigma_{ii}^{-}}, \quad \mathrm{F}_{ij} = \frac{1}{\tau_{ij}} \quad \text{and} \quad \mathrm{f}_i = \frac{1}{2}\left(\frac{1}{\sigma_{ii}^{+}} - \frac{1}{\sigma_{ii}^{-}}\right). \tag{5}$$

The uniaxial strengths in tension σ_{ii}^{+} and in compression σ_{ii}^{-} in the main directions are calculated with:

$$\sigma_{ii}^{+} = \sigma_0^{+} \rho^p \mathrm{m}_i^{2q}, \quad \sigma_{ii}^{-} = \sigma_0^{-} \rho^p \mathrm{m}_i^{2q} \tag{6}$$

where σ_0^{+} and σ_0^{-} are tissue yield stresses that correspond to a virtual case with $\rho = 1$ and $\mathbf{M} = \mathbf{I}$. The constants p and q are power coefficients. The interaction parameter ζ_{ij} of $\mathbb{F}$ and the shear strength τ_{ij} are calculated with:

$$\zeta_{ij} = \zeta_0 \frac{\mathrm{m}_i^{2q}}{\mathrm{m}_j^{2q}}, \quad \tau_{ij} = \tau_0 \rho^p \mathrm{m}_i^q \mathrm{m}_j^q \tag{7}$$

where ζ_0 is a stress interaction coefficient and τ_0 is the tissue shear strength. The parameters σ_0^+, σ_0^-, τ_0, ζ_0, p and q are obtained from the fitting procedure.

For representation of different samples, the stress tensor can be normalized with respect to fabric and density (Wolfram et al. 2012; Schwiedrzik et al. 2013):

$$\hat{\mathbf{S}} = \frac{\mathbf{M}^{-q}\mathbf{S}\mathbf{M}^{-q}}{\rho^p} \tag{8}$$

and the criterion can be written in normalized stress space as:

$$\mathrm{Y}(\hat{\mathbf{S}}) := \sqrt{\hat{\mathbf{S}} : \hat{\mathbb{F}}\hat{\mathbf{S}}} + \hat{\mathbf{F}} : \hat{\mathbf{S}} - 1 = 0 \tag{9}$$

where the tensors $\hat{\mathbb{F}}$ and $\hat{\mathbf{F}}$ exhibit cubic symmetry (Schwiedrzik et al. 2013) and become independent of volume fraction and fabric.

The yield criterion in strain space can be written in an analogous way as:

$$\mathrm{Y}(\mathbf{E}) := \sqrt{\mathbf{E} : \mathbb{G}\mathbf{E}} + \mathbf{G} : \mathbf{E} - 1 = 0 \tag{10}$$

where $\mathbf{E}$ is the infinitesimal strain tensor. The fourth-order tensor $\mathbb{G}$ and the second-order tensor $\mathbf{G}$ contain the model parameters.

The uniaxial ultimate strains in tension ε_{ii}^+ and in compression ε_{ii}^- are calculated with:

$$\varepsilon_{ii}^+ = \varepsilon_0^+ \rho^u \mathrm{m}_i^{2v}, \quad \varepsilon_{ii}^- = \varepsilon_0^- \rho^u \mathrm{m}_i^{2v} \tag{11}$$

where ε_0^+ and ε_0^- are tissue tensile and compressive yield strains, and u and v are power coefficients. The interaction parameter ξ_{ij} of $\mathbb{G}$ and the shear strain γ_{ij} are calculated with:

$$\xi_{ij} = \xi_0 \frac{\mathrm{m}_i^{2v}}{\mathrm{m}_j^{2v}}, \quad \gamma_{ij} = \gamma_0 \rho^u \mathrm{m}_i^v \mathrm{m}_j^v \tag{12}$$

where ξ_0 is a strain interaction coefficient, and γ_0 is the shear yield strain. The parameters ε_0^+, ε_0^-, γ_0, ξ_0, u and v are obtained from fitting procedure.

3 Materials and methods

Three proximal femora from two female donors (62 and 75) were studied. The bones were free of bone pathologies. Collection and preparation procedures were approved by the ethics commission of the Medical University of Vienna (Dall'Ara et al. 2013). Bone sections from the femoral heads were scanned with micro-computed tomography (μCT 40, SCANCO Medial AG, Brüttisellen, Switzerland) with a resolution of 18 μm. The scanning and extraction procedure is explained in detail by Dall'Ara et al. (2013).

Trabecular regions were cropped from these sections, and 167 cubic regions of interest (ROI) with a side length of 9.2 mm were obtained. Since PMUBCs require that the microstructures of the volumes of interest are aligned with the orthotropic symmetry planes, the ROIs were rotated iteratively so that the fabric tensor principal axes of an inner cubic subregion with 5.3-mm side length were aligned with its edges. The fabric tensor was evaluated by using the mean intercept length (MIL) method (Harrigan and Mann 1984; Whitehouse 1974). The degree of anisotropy (DA) equals the maximum fabric eigenvalue over the minimum fabric eigenvalue. A linear interpolation scheme was used in the image rotation. After rotation, cubic subregions with a side length of 5.3 mm were cropped, coarsened to a resolution of 36 μm, segmented by using a single-level threshold (Riedler and Calvard 1978) and cleaned by removing unconnected regions. Bone volume fraction (BV/TV) was computed by voxel counting. Then, μFE models were generated by converting directly the image voxels to eight-node linear hexahedral elements. Our previous study found that stiffness computed with PMUBCs is sensitive to heterogeneity. Accordingly, highly heterogeneous samples were excluded from the data set by using the coefficient of variation of BV/TV within each cubic biopsy as a criterion (Panyasantisuk et al. 2015). Each bone cube was divided equally into eight cubic subregions, and BV/TV was calculated for each subregion. The coefficient of variation equals the standard deviation over the mean of BV/TV. Bone cubes with coefficients of variation greater than 0.263 were excluded from the data set. The remaining 126 cubic subregions were used for homogenization analysis (Panyasantisuk et al. 2015) and reutilized in this study. The resulting data set has a mean BV/TV (±standard deviation, range) of 0.27 (±0.08, 0.12–0.40) and a mean DA of 1.57 (±0.18, 1.17–2.14).

Nonlinear μFE analyses of the trabecular bone cubes were performed by applying displacement-controlled KUBCs or PMUBCs with the parallel version of the FEAP (ParFEAP) software. For this purpose, 17 load cases (Table 1) including 3 uniaxial tension, 3 uniaxial compression, 3 shear and 8 multiaxial normal loading were applied on the trabecular bone samples (Wolfram et al. 2012). An isotropic elasto-plastic material model (Schwiedrzik and Zysset 2012) based on Green–Lagrange strain and the second Piola–Kirchhoff stress were used for tissue material. Each element was assigned an elastic modulus of 10 GPa (Schwiedrzik et al. 2015), a Poisson's ratio of 0.3, an approximated Drucker–Prager yield surface (Schwiedrzik et al. 2013) with tissue yield strain of 0.54 % in tension and 0.81 % in compression,

Table 1 Seventeen load cases tested on each trabecular bone sample. $\pm S_{ij}$ is applied stress in $\boldsymbol{e}_i \otimes \boldsymbol{e}_j$ direction where $i, j = 1, 2, 3$

l	$\boldsymbol{e}_1 \otimes \boldsymbol{e}_1$	$\boldsymbol{e}_2 \otimes \boldsymbol{e}_2$	$\boldsymbol{e}_3 \otimes \boldsymbol{e}_3$	$\boldsymbol{e}_1 \otimes \boldsymbol{e}_2$	$\boldsymbol{e}_1 \otimes \boldsymbol{e}_3$	$\boldsymbol{e}_2 \otimes \boldsymbol{e}_3$
1	$+S_{11}$	–	–	–	–	–
2	–	$+S_{22}$	–	–	–	–
3	–	–	$+S_{33}$	–	–	–
4	$-S_{11}$	–	–	–	–	–
5	–	$-S_{22}$	–	–	–	–
6	–	–	$-S_{33}$	–	–	–
7	–	–	–	$-S_{12}$	–	–
8	–	–	–	–	$-S_{13}$	–
9	–	–	–	–	–	$-S_{23}$
10	$+S_{11}$	$+S_{22}$	$+S_{33}$	–	–	–
11	$-S_{11}$	$+S_{22}$	$+S_{33}$	–	–	–
12	$+S_{11}$	$-S_{22}$	$+S_{33}$	–	–	–
13	$+S_{11}$	$+S_{22}$	$-S_{33}$	–	–	–
14	$+S_{11}$	$-S_{22}$	$-S_{33}$	–	–	–
15	$-S_{11}$	$+S_{22}$	$-S_{33}$	–	–	–
16	$-S_{11}$	$-S_{22}$	$+S_{33}$	–	–	–
17	$-S_{11}$	$-S_{22}$	$-S_{33}$	–	–	–

a linear hardening of 5 % of the elastic modulus and an interaction parameter of 0.49 (Gross 2014; Schwiedrzik et al. 2015).

Image processing and FE model generation were done with the software MEDTOOL (Dr. Pahr Ingenieurs e.U, Austria).

The applied displacement of each load case was related to a unit stress direction $\tilde{\mathbf{S}}^l$ of that load case where $l = 1,\ldots,17$ is load case number (Wolfram et al. 2012), as shown in Table 1. For example, the unit stress direction of the triaxial tension load case ($l = 10$) was given by:

$$\tilde{\mathbf{S}}^{10} = \frac{1}{\sqrt{3}}(\boldsymbol{e}_1 \otimes \boldsymbol{e}_1 + \boldsymbol{e}_2 \otimes \boldsymbol{e}_2 + \boldsymbol{e}_3 \otimes \boldsymbol{e}_3) \tag{13}$$

Subsequently, a unit strain tensor $\tilde{\mathbf{E}}^l$ associated with the unit stress direction $\tilde{\mathbf{S}}^l$ was calculated with:

$$\tilde{\mathbf{E}}^l = \frac{\mathbb{E}\tilde{\mathbf{S}}^l}{\|\mathbb{E}\tilde{\mathbf{S}}^l\|} \tag{14}$$

where $\mathbb{E}$ is the anisotropic compliance tensor. For progressive application of the load cases, the unit strain tensor $\tilde{\mathbf{E}}^l$ was amplified with a coefficient λ to obtain a small-strain tensor $\mathbf{E}^l$.

$$\mathbf{E}^l = \lambda\tilde{\mathbf{E}}^l \tag{15}$$

Displacements based on $\mathbf{E}^l$ were applied on boundaries according to KUBCs and PMUBCs, which are explained in detail by Pahr and Zysset (2008). From the output of the μFE simulations, the apparent Cauchy stress tensor $\mathbf{S}^l_{\mathrm{FE}}$ of each trabecular bone sample was calculated by using the stress volume averages (Pahr and Zysset 2008). The apparent stress $\mathbf{S}^l_{\mathrm{FE}}$ is then projected to the assigned stress direction $\tilde{\mathbf{S}}^l$ to calculate a projected stress S^l_{FE}.

$$S^l_{\mathrm{FE}} = \mathbf{S}^l_{\mathrm{FE}} : \tilde{\mathbf{S}}^l \tag{16}$$

The yield stress ${}^{\mathrm{y}}S^l_{\mathrm{FE}}$ and yield strain ${}^{\mathrm{y}}E^l_{\mathrm{FE}}$ were determined by using a 0.2 % offset of the projected stress S^l_{FE} and strain norm $\|\mathbf{E}^l\| = \sqrt{\mathbf{E}^l : \mathbf{E}^l}$. The computed ${}^{\mathrm{y}}S^l_{\mathrm{FE}}$ of KUBCs and PMUBCs were compared in a one-to-one relationship. A normalized error $\mathrm{NE}_{\mathrm{KUBC-PMUBC}}$ describes the difference in ${}^{\mathrm{y}}S^l_{\mathrm{FE}}$ between the two BCs in percent:

$$\mathrm{NE}_{\mathrm{KUBC-PMUBC}} = 100 \cdot \frac{{}^{\mathrm{y}}S^l_{\mathrm{KUBC}} - {}^{\mathrm{y}}S^l_{\mathrm{PMUBC}}}{{}^{\mathrm{y}}S^l_{\mathrm{PMUBC}}} \tag{17}$$

The predicted yield stress ${}^{\mathrm{y}}S^l_{\mathrm{QC}}$ can be extracted from the yield criterion using the direction $\tilde{\mathbf{S}}^l$:

$${}^{\mathrm{y}}S^l_{\mathrm{QC}} = \frac{1}{\sqrt{\tilde{\mathbf{S}}^l : \mathbb{F}\tilde{\mathbf{S}}^l} + \mathbf{F} : \tilde{\mathbf{S}}^l} \tag{18}$$

The error between computed ${}^{\mathrm{y}}S^l_{\mathrm{FE}}$ and predicted ${}^{\mathrm{y}}S^l_{\mathrm{QC}}$ was minimized in the log space:

$$\mathrm{Min}_{\{\sigma_0^+,\sigma_0^-,\tau_0,\zeta_0,p,q\}}\left(\sum_{n=1}^{N}\sum_{l=1}^{LC}(\ln({}^{\mathrm{y}}S^l_{\mathrm{FE},n}) - \ln({}^{\mathrm{y}}S^l_{\mathrm{QC},n}))^2\right) \tag{19}$$

N is the number of samples and LC is the number of load cases. Firstly, the KUBC-based and PMUBC-based yield stresses were fitted to the quadric yield function separately to obtain two individual sets of fitting parameters. The variation between ${}^{\mathrm{y}}S^l_{\mathrm{FE}}$ and ${}^{\mathrm{y}}S^l_{\mathrm{QC}}$ is expressed by the normalized error $\mathrm{NE}_{\mathrm{FE-QC}}$ in percent:

$$\mathrm{NE}_{\mathrm{FE-QC}} = 100 \cdot \sqrt{\frac{\sum_{n=1}^{N}\sum_{l=1}^{LC}({}^{\mathrm{y}}S^l_{\mathrm{FE},n} - {}^{\mathrm{y}}S^l_{\mathrm{QC},n})^2}{\sum_{n=1}^{N}\sum_{l=1}^{LC}({}^{\mathrm{y}}S^l_{\mathrm{FE},n})^2}} \tag{20}$$

For the comparison of σ_0^+, σ_0^-, τ_0 and ζ_0 between KUBCs and PMUBCs, a minimization was then performed so that the two BCs share the same exponents p and q. Furthermore, the pooled KUBC-based and PMUBC-based yield stresses were fitted to obtain a single set of the six fitting parameters. Similarly, yield strains were fitted to the quadric criterion in strain space. Figure 1 summarizes the nonlinear analysis methodology of the current study showing the triaxial tension load case and a comparison between yield surfaces of KUBCs and PMUBCs in stress space.

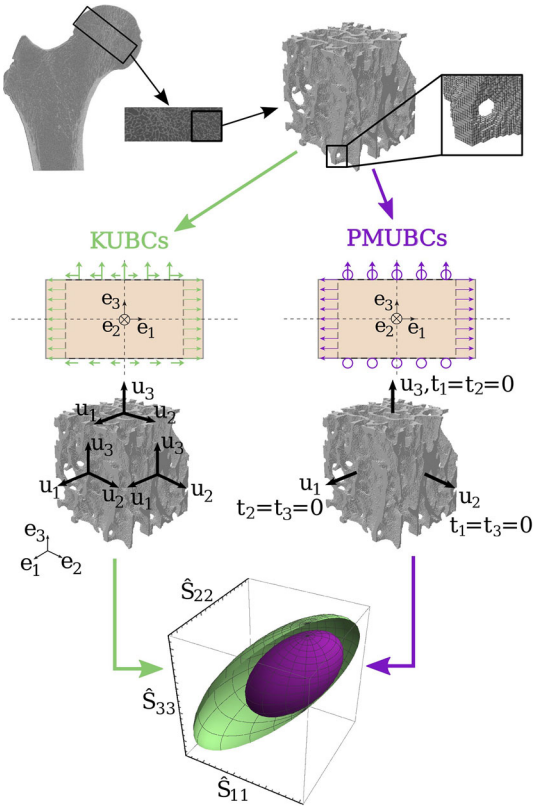

Fig. 1 Nonlinear analysis methodology of femoral trabecular bone cubic specimens comparing yield surfaces of KUBCs and PMUBCs in stress space. The variables u_i, t_i, $\mathbf{e}_i$ and $\hat{S}_{ij}$ are displacements, tractions, unit directions and normalized stress tensor components, respectively

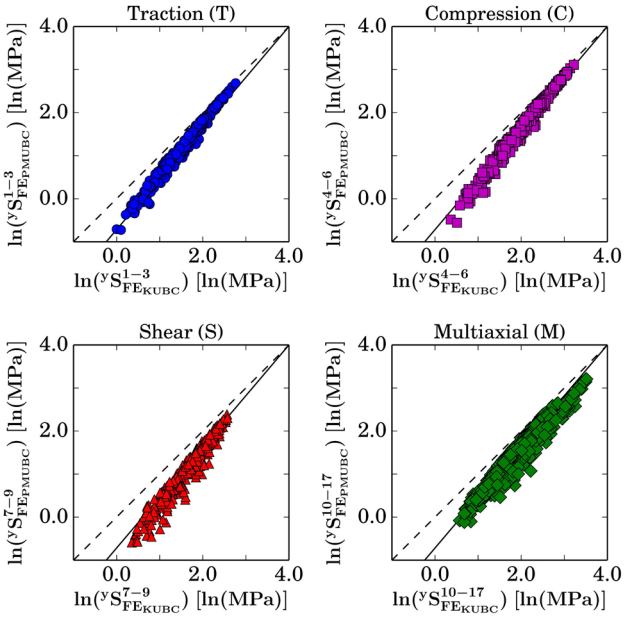

Fig. 2 Comparison of μFE yield stresses based on KUBCs and PMUBCs in the log space. The global regression of all 17 load cases illustrated by the *solid lines*. PMUBCs lead to lower yield stresses compared to KUBCs

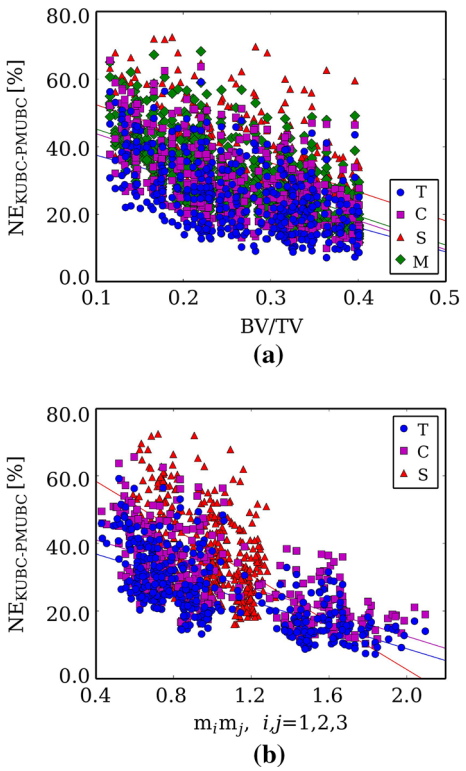

Fig. 3 **a** Relationship of the difference $NE_{KUBC-PMUBC}$ and BV/TV: $NE_{KUBC-PMUBC}$ decreases with increasing BV/TV. Shear yield stresses have the highest difference; **b** the relationship of $NE_{KUBC-PMUBC}$ and fabric: $NE_{KUBC-PMUBC}$ decreases with increasing fabric eigenvalues. T, C, S and M denote traction, compression, shear and multiaxial load cases. The regression slopes were found to be significantly lower than zero for all load case groups

4 Results

4.1 Stress space

PMUBCs lead to lower homogenized yield stresses compared to KUBCs but the two BCs are linearly related in the log space. Figure 2 shows the relationship between KUBC-based and PMUBC-based yield stresses. The global regression equation reads $y = 1.18x - 0.72$ with a coefficient of determination (r^2) of 0.95 and SEE of 0.006. Yield stresses of the two BCs have a concordance correlation coefficient (r^c) of 0.82. As Fig. 3 reveals, the difference $NE_{KUBC-PMUBC}$ decreases with increasing BV/TV and increasing fabric eigenvalues. Linear regressions confirm that the decrease is highly significant for all load case groups ($p < 0.001$). The ranges of $NE_{KUBC-PMUBC}$ are 7–59 % for traction, 10–66 % for compression, 16–72 % for shear and 12–68 % for multiaxial load cases.

The quadric yield criterion successfully fitted both KUBC-based and PMUBC-based yield stresses. Table 2 shows the homogenized fitting parameters in stress space. Sets 1 and 2 were obtained from fitting separately yield stresses of KUBCs and PMUBCs, respectively. PMUBC-based expo-

Table 2 Quadric yield criterion parameters, standard errors of the estimate and coefficients of determination obtained by fitting (1) KUBC-based yield stresses separately, (2) PMUBC-based yield stresses separately, (3) pooled KUBC-based and PMUBC-based yield stresses so that only the exponents p and q are shared between the two parameter sets, and (4) pooled KUBC-based and PMUBC-based yield stresses

Set		σ_0^+	σ_0^-	τ_0	ζ_0	p	q	SEE	r^2
1	KUBCs	49.00	64.57	31.11	0.30	1.50	0.71	0.005	0.95
2	PMUBCs	57.69	73.10	29.61	0.28	1.82	0.98	0.006	0.93
3	KUBCs	62.37	82.09	39.04	0.32	1.66	0.85	0.004	0.93
	PMUBCs	45.25	57.42	23.60	0.26				
4	KUBCs and PMUBCs	53.12	68.70	30.36	0.29	1.66	0.85	0.006	0.85

nents p and q (Set 2) are 20% and 38% higher than those of KUBCs (Set 1). Sets 3 and 4 were obtained from pooled yield stresses of KUBCs and PMUBCs. In Set 3, KUBCs and PMUBCs share the same exponents p and q, but have separate sets of σ_0^+, σ_0^-, τ_0 and ζ_0, which are substantially higher in KUBCs than in PMUBCs. The differences with respect to PMUBCs are 38, 42 and 65 % for σ_0^+, σ_0^- and τ_0, respectively. Set 4 is an average over yield stresses of the two BCs.

Figure 4 shows the linear regressions of the relationship between the predicted ${}^{y}S_{QC}^{l}$ and computed ${}^{y}S_{FE}^{l}$ based on KUBCs (Fig. 4a) and PMUBCs (Fig. 4b) in which the predicted ${}^{y}S_{QC}^{l}$ were calculated by using the parameters in Sets 1 and 2, respectively.

Yield surfaces based on the parameters in Set 3 were illustrated in 3D and 2D as seen in Figs. 5 and 6, respectively. The two yield surfaces have a pressure-sensitive ellipsoidal shape. The amplitude of the KUBC-based yield surface is 37–84 % larger than the PMUBC-based one, and the largest difference is in the hydrostatic direction.

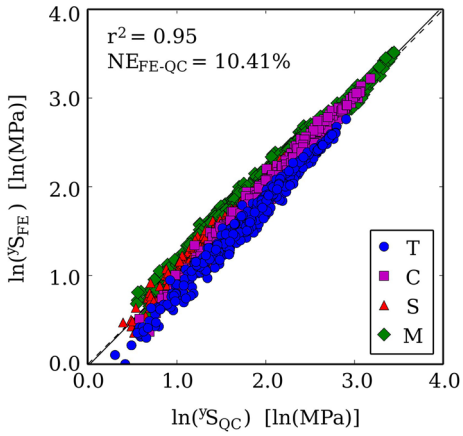

(a) KUBCs

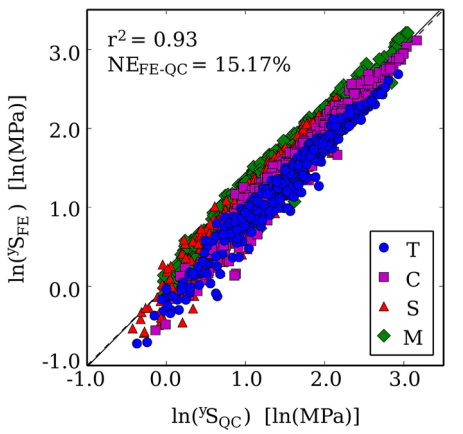

(b) PMUBCs

Fig. 4 Linear regressions of the relationship between the μFE and predicted yield stresses calculated by using the fitting parameters in **a** Set 1 for KUBCs and **b** Set 2 for PMUBCs. T, C, S and M denote traction, compression, shear and multiaxial load cases

4.2 Strain space

Yield strains have lower variations compared to yield stresses. Figure 7 shows the relationship between KUBC-based and PMUBC-based yield strains in the log space. The global regression equation is $y = x - 0.04$. The regression has r^2 of 0.88 and SEE of 0.009. The two BCs have a concordance r^c of 0.91.

Yield strains were also fitted to the quadric yield criterion. Table 3 shows fitting parameters, Sets 5–8, which were obtained by fitting yield strains of KUBCs (Set 5) and PMUBCs (Set 6) separately, pooled yield strains of KUBCs and PMUBCs so that they share the same exponents u and v (Set 7), and pooled yield strains of the two BCs (Set 8). These sets are analogous to Sets 1–4 in stress space. All ξ_0 and the exponents u and v are negative. The magnitude of the exponents u are 21–26 times lower than the exponents p of the associated sets in stress space. Similarly, the exponents v are 4–5 times lower than the exponents q of the associated sets in stress space. PMUBC-based exponents u and v (Set 6) are 51 and 19 % higher than those of KUBCs (Set 5). In Set 7, γ_0 is equal in KUBCs and PMUBCs, while ε_0^+ and ε_0^- in KUBCs are 2 and 10 % higher than in PMUBCs, respectively.

Figures 8 and 9 illustrate 3D and 2D plots of yield surfaces using the parameter in Set 7, respectively. The yield surfaces have a volume-sensitive ellipsoidal shape. The amplitude

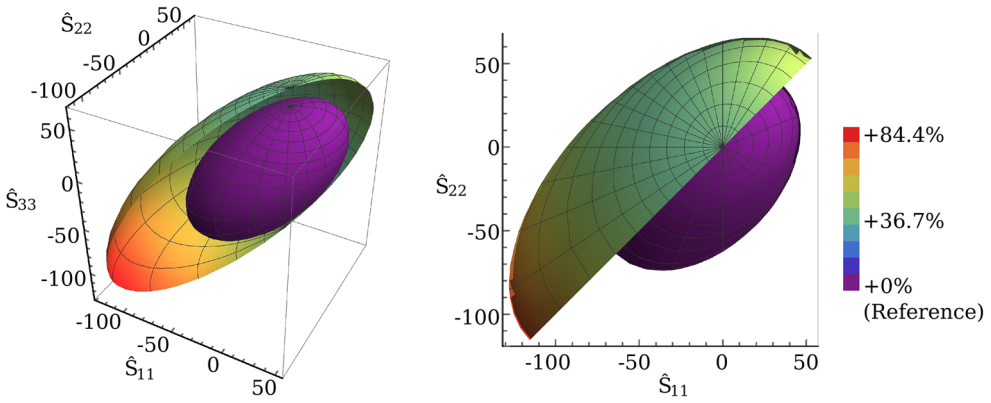

Fig. 5 Yield surfaces of KUBCs (outer surface) and PMUBCs (inner surface) colored by the ratios of yield stresses of KUBCS over PMUBCs in 3D view (*left*) and top view (*right*) using the fitting parameter Set 3 in which KUBCs and PMUBCs share the same exponent p and q

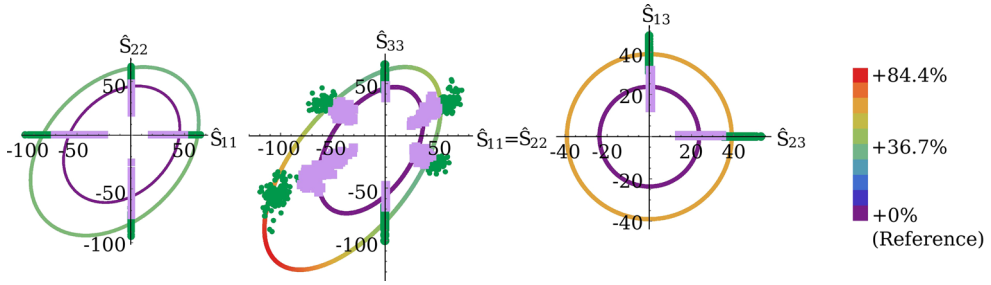

Fig. 6 Cross sections of yield surfaces in normalized stress space at the plane $\hat{S}_{33} = 0$ (*left*), $\hat{S}_{11} = \hat{S}_{22}$ (*center*) and $\hat{S}_{12} = 0$ (*right*). Normalized yield stresses of KUBCs (*dots*) and PMUBCs (*squares*) were projected to the nearest planes for multiaxial cases

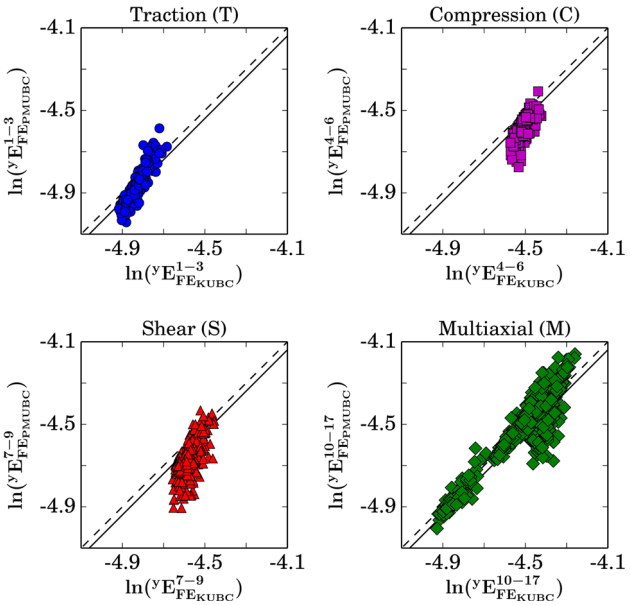

Fig. 7 Comparison of μFE yield strains based on KUBCs and PMUBCs in the log space. The global regression of all 17 load cases illustrated by the *solid lines*

of KUBC-based yield surface is 1–19 % larger than that of PMUBCs and the largest difference along the trisectrix.

5 Discussion

The aim of this study was to evaluate and compare the homogenized yield properties of human femoral trabecular bone obtained by applying KUBCs and PMUBCs on a large number of loading directions and μFE models. Seventeen load cases were investigated, and a total set of 126 femoral trabecular cubic biopsies covered a broad BV/TV range of 0.12–0.40 and a DA range of 1.17–2.14.

The normalized yield surface and therefore all yield surfaces of the individual samples are pressure-dependent (Figs. 5 and 8) as shown by Rincón-Kohli and Zysset (2008) and confirmed by Kelly and McGarry (2012). The ellipsoidal shape of the yield envelope resulted in $\zeta_0 < \zeta_{0,crit}$ as described by Schwiedrzik et al. (2013).

The quadric yield function successfully fitted both BCs in stress space with $r^c \geq 0.96$ and $NE_{FE-QC} < 15\,\%$. The exponent of volume fraction p ranges from 1.50 to 1.82 and is bounded by the power coefficient of 2 for apparent density in the statistical analysis of uniaxial data by Rice et al. (1988). The KUBC-based exponent $p = 1.50$ is higher than 1.28 obtained in Rincón-Kohli and Zysset (2008)'s experimental study in which yield stresses of uniaxial tension, uniaxial compression and multiaxial compression experiments were fitted to a BV/TV and fabric-based model. However, the

Table 3 Quadric yield criterion parameters, standard errors of the estimate and coefficients of determination obtained by fitting (5) KUBC-based yield strains separately, (6) PMUBC-based yield strains separately, (7) pooled KUBC-based and PMUBC-based yield strains so that only the exponents u and v are shared between the two parameter sets, and (8) pooled KUBC-based and PMUBC-based yield strains

Set		ε_0^+	ε_0^-	γ_0	ξ_0	u	v	SEE	r^2
5	KUBCs	7.37e−3	10.76e−3	13.29e−3	−0.151	−0.057	−0.180	0.015	0.65
6	PMUBCs	6.86e−3	9.40e−3	11.65e−3	−0.216	−0.086	−0.215	0.019	0.53
7	KUBCs	7.18e−3	10.50e−3	11.93e−3	−0.155	−0.072	−0.203	0.012	0.59
	PMUBCs	7.02e−3	9.57e−3	11.93e−3	−0.215				
8	KUBCs and PMUBCs	7.12e−3	10.06e−3	12.45e−3	−0.179	−0.073	−0.198	0.013	0.56

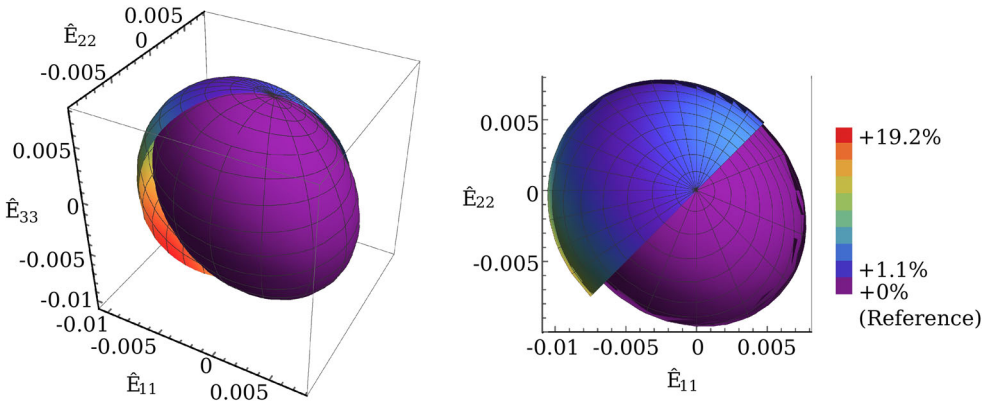

Fig. 8 Yield surfaces of KUBCs (outer surface) and PMUBCs (inner surface) colored by the ratio of yield strain of KUBCS over PMUBCs in 3D view (*left*) and top view (*right*) using the fitting parameter Set 7 in which KUBCs and PMUBCs share the same exponent u and v

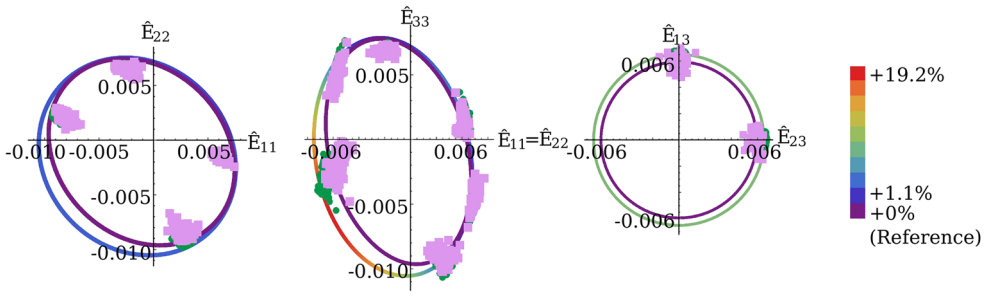

Fig. 9 Cross sections of yield surfaces in normalized strain space at the plane $\hat{E}_{33} = 0$ (*left*), $\hat{E}_{11} = \hat{E}_{22}$ (*center*) and $\hat{E}_{12} = 0$ (*right*). Normalized yield strains of KUBCs (*dots*) and PMUBCs (*squares*) were projected to the nearest planes for multiaxial cases

KUBC-based exponent p agrees well with 1.5 of idealized open cell models (Zysset et al. 1999) and 1.51 obtained from uniaxial compressive mechanical tests of Matsuura et al. (2008).

The same morphology–yield behavior was found in Wolfram et al. (2012), in which a Tsai–Wu criterion was identified, and Rincón-Kohli and Zysset (2008), in which a piecewise Hill model was used.

The amplitude of the KUBC-based yield surface reported here seems larger than the one obtained in the study of Wolfram et al. (2012) in which vertebral trabecular bone samples with a BV/TV range of 0.06–0.15 were investigated. However, in the corresponding BV/TV range of 0.11–0.15, the fitting parameters of the femoral and vertebral trabecular bone specimens correspond better as shown in Table 4. In this BV/TV range, the amplitude of the yield surface of the femoral data is 7–42 % larger than that of the vertebral, and the largest difference is found in the triaxial tension direction. This may correspond to the higher misalignment of the main axis to the global axis in the vertebral data set. Applying tensile loading on misaligned microstructures generates off-axis loading and leads to lower yield stresses compared to applying the same loading on carefully aligned microstructures such as the femoral data set. Moreover, Wolfram et al. used the cast iron plasticity model, which is slightly different from the tissue plasticity model used in this study.

Table 4 Quadric yield criterion fitting parameters, standard errors of the estimate, coefficients of determination and number of samples of Wolfram et al. (2012) and the current study; the fitting parameters of the two studies correspond better at the same BV/TV range (0.11–0.15)

	σ_0^+	σ_0^-	τ_0	ζ_0	p	q	SEE	r^2	n
Wolfram et al. (2012) Full BV/TV range	64.28	91.15	40.08	0.28	1.72	0.89	0.015	0.90	23
Wolfram et al. (2012) BV/TV 0.11–0.15	34.12	48.13	21.84	0.30	1.41	0.86	0.026	0.85	14
The current study BV/TV 0.11–0.15	35.22	44.61	21.97	0.31	1.34	0.82	0.04	0.86	7

In stress space, PMUBCs lead to remarkably lower yield stresses with 7–72 % difference compared to KUBCs, which are known as an upper bound to all apparent stiffness tensors (Hazanov and Huet 1994; Pahr and Zysset 2008). As shown in previous studies, KUBCs indeed lead to higher elastic constants than PMUBCs (Pahr and Zysset 2008; Panyasantisuk et al. 2015). The difference in yield stresses between the two BCs decreases with increasing BV/TV and fabric eigenvalues. This trend was also found for elastic constants (Panyasantisuk et al. 2015) and confirms the importance of the BCs in the apparent mechanical behavior of human trabecular bone.

In strain space, the yield surfaces are also closed and the apparent yield strains have small variations. As expected from the literature, yield strains showed only a weak dependency on BV/TV and fabric ($r^2 = 0.53-0.65$). Yield strains decrease with increasing BV/TV and fabric eigenvalues as expressed by the negative power u and v. In KUBCs, mean yield strains ($\pm$ standard deviation) are 1.09 %($\pm$0.02 %) in uniaxial compression along the principal trabecular direction and 0.79 %($\pm$0.02 %) in uniaxial tension in the same principal direction. Compared to published experimental results, these values are in the high range of Gross (2014)'s results and higher than those in Matsuura et al. (2008) and Morgan and Keaveny (2001). This overestimation in the apparent level may well be due to the higher yield strains and the fully ductile behavior assumed at the tissue level. In fact, the compressive yield strain used in our study (0.81 %) is identical as in other μFE studies, but our tensile yield strains (0.54 %) are 64 % higher than in previous μFE studies (Bevill et al. 2006), which delays the onset of yield at the apparent level in both tensile and compressive modes. In a recent study, Nawathe et al. (2013) showed that apparent yield strains computed by μFE are an upper bound for the experimental ones. They showed in particular that, at low BV/TV (<0.20), experimental apparent yield strains are in between the fully ductile and fully brittle μFE apparent yield strains. On the contrary, at high BV/TV (>0.20), the experimental apparent yield strains agree well with the μFE apparent yield strains.

Sanyal et al. (2015) introduced a quartic piecewise-linear (QPL) yield criterion with which, however, results of the current study cannot be compared directly because of the following differences. First, the definition of yield stress and strain is different. In their study, for each load case, stress–strain curves were obtained in each material direction, and yield points were acquired for each material direction. From these yield points, the point that occurred first among the 1-, 2- and 3-material directions was defined as the yield point of that load case. Subsequently, yield stresses and strains of multiaxial load cases were normalized by the uniaxial yield stresses and strains, respectively. In the current study, for each load case, only one stress–strain curve was obtained and was defined as a relationship of a projected stress and a strain norm along an elastic direction. A yield point was obtained from this curve and used directly in the minimization. Second, the definition of anisotropy is different. Sanyal et al. used mechanical anisotropy ratios from the apparent elastic moduli instead of the fabric eigenvalues used in the present study. Third, a normal–shear load case tested by Sanyal et al. was not included in the current study. Under the assumption of orthotropic symmetry, the off-axis terms are zero in the quadratic form describing yield and no interaction is expected. Fourth, the quadric yield criterion cannot describe a box-like shape. However, it was shown in the result section (Figs. 6, 9) that the quadric yield surfaces successfully captured yield stresses and strains for 17 load cases with our general definition of yield. Moreover, the quadric yield criterion is defined with only 6 parameters, whereas the QPL criterion requires up to 22 coefficients.

The amplitude of the normalized yield surfaces of KUBCs and PMUBCs were compared. In stress space, a large difference (37–84 %) was observed, whereas a small difference (1–19 %) was found in strain space. In both spaces, the largest difference lay along the direction of hydrostatic pressure. This relates to the fact that, under KUBCs, every node on the boundaries is constrained with homogeneous displacements in all directions. This delays excessive bending and subsequent localization to occur in microstructures in compression, especially in hydrostatic compression. The difference in triaxial tension is lower than that in triaxial compression because the assigned tissue yield strain in tension is lower than in compression.

There are some limitations in this study. First, only two female donors were included. However, Homminga et al. (2003) used μFE to compute the elastic properties of trabecular bone samples from numerous patients with ($n = 26$) and without ($n = 32$) hip fracture and found a unique morphology–elasticity relationship for all samples. This

indicates that the number of donors and the presence of osteoporosis do not play a role and that the morphology–mechanical property relationships of human trabecular bone may well be universal. Second, tissue behavior was assigned to be fully ductile, which was shown to overestimate the experimental yield properties, especially at low BV/TV (Nawathe et al. 2013). Interestingly, the apparent yield properties derived from the fully ductile and fully brittle material properties are highly correlated (Nawathe et al. 2013), but the influence of these post-yield properties on the shape of the yield surface remains unknown. Third, there are only few experimental results for validation. Currently available experimental results on human bone include only uniaxial, torsion and a few combined load cases (Morgan and Keaveny 2001; Rincón-Kohli and Zysset 2008; Matsuura et al. 2008). Experiments rely on complex setups and are limited to relatively simple load cases, and each sample can only be tested once in the yield region. Experiments also suffer from multiple boundary artefacts (Keaveny et al. 1997) and different surfaces of a sample have different BCs. The adopted μFE approach offers therefore a unique opportunity to apply multiple load cases on numerous samples with well-defined BCs.

This study characterized the influence of KUBCs and PMUBCs on homogenized yield properties of human trabecular bone for the first time. Moreover, it includes 126 samples representing a wide range of trabecular bone morphology. In future studies, the apparent elastic and yield properties obtained with the two BCs will need to be explored with homogenized FE analysis at the whole bone level. KUBCs provide an upper bound to the apparent stiffness and yield behavior. They may be suitable for trabecular bone regions with a stiff surrounding such as regions near the cortex. On the other hand, PMUBCs provide more compliant elasticity and yield properties. They may represent the behavior of a trabecular volume element that is surrounded by a similar trabecular morphology with similar rigidity. The knowledge of trabecular yield behavior gained from this study is therefore expected to help generate more accurate homogenized FE models of whole bones and bone-implant systems, and improve accuracy of bone fracture risk assessment and implant stability prediction.

Acknowledgments The authors would like to thank Dr. Uwe Wolfram for the helpful guidance in postprocessing and Dr. Markus Bina for setting up the ParFEAP software.

References

Bayraktar HH, Gupta A, Kwon RY, Papadopoulos P, Keaveny TM (2005) The modified super-ellipsoid yield criterion for human trabecular bone. J Biomech Eng 126(6):677–684. doi:10.1115/1.1763177

Bevill G, Eswaran SK, Gupta A, Papadopoulos P, Keaveny TM (2006) Influence of bone volume fraction and architecture on computed large-deformation failure mechanisms in human trabecular bone. Bone 39(6):1218–1225. doi:10.1016/j.bone.2006.06.016

Cowin SC (1985) The relationship between the elasticity tensor and the fabric tensor. Mech Mater 4(2):137–147. doi:10.1016/0167-6636(85)90012-2

Dall'Ara E, Pahr D, Varga P, Kainberger F, Zysset P (2012) QCT-based finite element models predict human vertebral strength in vitro significantly better than simulated DEXA. Osteoporos Int 23(2):563–572. doi:10.1007/s00198-011-1568-3

Dall'Ara E, Luisier B, Schmidt R, Kainberger F, Zysset P, Pahr D (2013) A nonlinear QCT-based finite element model validation study for the human femur tested in two configurations in vitro. Bone 52(1):27–38. doi:10.1016/j.bone.2012.09.006

Gross T (2014) Development and application of 3d CT image-based micro and macro finite element models for human bones and orthopedic implant systems. In: PhD thesis, Vienna University of Technology

Harrigan TP, Mann RW (1984) Characterization of microstructural anisotropy in orthotropic materials using a second rank tensor. J Mater Sci 19(3):761–767. doi:10.1007/BF00540446

Harrigan TP, Jasty M, Mann RW, Harris WH (1988) Limitations of the continuum assumption in cancellous bone. J Biomech 21(4):269–275. doi:10.1016/0021-9290(88)90257-6

Hazanov S, Amieur M (1995) On overall properties of elastic heterogeneous bodies smaller than the representative volume. Int J Eng Sci 33(9):1289–1301. doi:10.1016/0020-7225(94)00129-8

Hazanov S, Huet C (1994) Order relationships for boundary conditions effect in heterogeneous bodies smaller than the representative volume. J Mech Phys Solids 42(12):1995–2011. doi:10.1016/0022-5096(94)90022-1

Homminga J, Mccreadie BR, Weinans H, Huiskes R (2003) The dependence of the elastic properties of osteoporotic cancellous bone on volume fraction and fabric. J Biomech 36(10):1461–1467. doi:10.1016/S0021-9290(03)00125-8

Keaveny TM, Pinilla TP, Crawford RP, Kopperdahl DL, Lou A (1997) Systematic and random errors in compression testing of trabecular bone. J Orthop Res 15(1):101–110. doi:10.1002/jor.1100150115

Keaveny TM, Wachtel EF, Zadesky SP, Arramon YP (1999) Application of the Tsai–Wu quadratic multiaxial failure criterion to bovine trabecular bone. J Biomech Eng 121(1):99–107. doi:10.1115/1.2798051

Kelly N, McGarry JP (2012) Experimental and numerical characterisation of the elasto-plastic properties of bovine trabecular bone and a trabecular bone analogue. J Mech Behav Biomed Mater 9:184–197. doi:10.1016/j.jmbbm.2011.11.013

MacNeil JA, Boyd SK (2008) Bone strength at the distal radius can be estimated from high-resolution peripheral quantitative computed tomography and the finite element method. Bone 42(6):1203–1213. doi:10.1016/j.bone.2008.01.017

Matsuura M, Eckstein F, Lochmüller EM, Zysset PK (2008) The role of fabric in the quasi-static compressive mechanical properties of human trabecular bone from various anatomical locations. Biomech Model Mechanobiol 7(1):27–42. doi:10.1007/s10237-006-0073-7

Morgan EF, Keaveny TM (2001) Dependence of yield strain of human trabecular bone on anatomic site. J Biomech 34(5):569–577. doi:10.1016/S0021-9290(01)00011-2

Nawathe S, Juillard F, Keaveny TM (2013) Theoretical bounds for the influence of tissue-level ductility on the apparent-level strength of human trabecular bone. J Biomech 46(7):1293–1299. doi:10.1016/j.jbiomech.2013.02.011

Niebur GL, Feldstein MJ, Yuen JC, Chen TJ, Keaveny TM (2000) High-resolution finite element models with tissue strength asym-

metry accurately predict failure of trabecular bone. J Biomech 33(12):1575–1583. doi:10.1016/S0021-9290(00)00149-4
Niebur GL, Feldstein MJ, Keaveny TM (2002) Biaxial failure behavior of bovine tibial trabecular bone. J Biomech Eng 124(6):699–705
Ostoja-Starzewski M (2006) Material spatial randomness: from statistical to representative volume element. Probab Eng Mech 21(2):112–132. doi:10.1016/j.probengmech.2005.07.007
Pahr D, Zysset P (2008) Influence of boundary conditions on computed apparent elastic properties of cancellous bone. Biomech Model Mechanobiol 7(6):463–476
Panyasantisuk J, Pahr DH, Gross T, Zysset PK (2015) Comparison of mixed and kinematic uniform boundary conditions in homogenized elasticity of femoral trabecular bone using microfinite element analyses. J Biomech Eng 137(1):011002. doi:10.1115/1.4028968
Rice JC, Cowin SC, Bowman JA (1988) On the dependence of the elasticity and strength of cancellous bone on apparent density. J Biomech 21(2):155–168. doi:10.1016/0021-9290(88)90008-5
Riedler TW, Calvard S (1978) Picture thresholding using an iterative selection method. IEEE Trans Syst Man Cybern 8(8):630–632. doi:10.1109/TSMC.1978.4310039
Rincón-Kohli L, Zysset PK (2008) Multi-axial mechanical properties of human trabecular bone. Biomech Model Mechanobiol 8(3):195–208. doi:10.1007/s10237-008-0128-z
Sambrook P, Cooper C (2006) Osteoporosis. The Lancet 367(9527):2010–2018. doi:10.1016/S0140-6736(06)68891-0
Sanyal A, Scheffelin J, Keaveny TM (2015) The quartic piecewise-linear criterion for the multiaxial yield behavior of human trabecular bone. J Biomech Eng. doi:10.1115/1.4029109
Schwiedrzik J, Gross T, Bina M, Pretterklieber M, Zysset P, Pahr D (2015) Experimental validation of a nonlinear FE model based on cohesive-frictional plasticity for trabecular bone. Int J Numer Methods Biomed Eng. doi:10.1002/cnm.2739
Schwiedrzik JJ, Zysset PK (2012) An anisotropic elastic-viscoplastic damage model for bone tissue. Biomech Model Mechanobiol 12(2):201–213. doi:10.1007/s10237-012-0392-9
Schwiedrzik JJ, Wolfram U, Zysset PK (2013) A generalized anisotropic quadric yield criterion and its application to bone tissue at multiple length scales. Biomech Model Mechanobiol. doi:10.1007/s10237-013-0472-5
Steiner JA, Ferguson SJ, van Lenthe GH (2015) Computational analysis of primary implant stability in trabecular bone. J Biomech 48(5):807–815. doi:10.1016/j.jbiomech.2014.12.008
Stölken JS, Kinney JH (2003) On the importance of geometric nonlinearity in finite-element simulations of trabecular bone failure. Bone 33(4):494–504. doi:10.1016/S8756-3282(03)00214-X
Verhulp E, van Rietbergen B, Müller R, Huiskes R (2008) Indirect determination of trabecular bone effective tissue failure properties using micro-finite element simulations. J Biomech 41(7):1479–1485. doi:10.1016/j.jbiomech.2008.02.032
Whitehouse WJ (1974) The quantitative morphology of anisotropic trabecular bone. J Microsc 101(2):153–168. doi:10.1111/j.1365-2818.1974.tb03878.x
Wolfram U, Gross T, Pahr DH, Schwiedrzik J, Wilke HJ, Zysset PK (2012) Fabric-based Tsai–Wu yield criteria for vertebral trabecular bone in stress and strain space. J Mech Behav Biomed Mater 15:218–228. doi:10.1016/j.jmbbm.2012.07.005
World Health Organization (2003) Prevention and management of osteoporosis. World Health Organization Technical Report Series, vol 921, pp 1–164, back cover
Zysset PK, Ominsky MS, Goldstein SA (1999) A novel 3d microstructural model for trabecular. Comput Methods Biomech Biomed Eng 2(1):1–11. doi:10.1080/10255849908907974